

# Probing quantum phases in ultra-high-mobility two-dimensional electron systems using surface acoustic waves

Mengmeng Wu,<sup>1</sup> Xiao Liu,<sup>1</sup> Renfei Wang,<sup>1</sup> Yoon Jang Chung,<sup>2</sup> Adbhut Gupta,<sup>2</sup> Kirk W. Baldwin,<sup>2</sup> Loren Pfeiffer,<sup>2</sup> Xi Lin,<sup>1,3,\*</sup> and Yang Liu<sup>1,†</sup>

<sup>1</sup>International Center for Quantum Materials, Peking University, Haidian, Beijing, 100871, China

<sup>2</sup>Department of Electrical Engineering, Princeton University, Princeton, New Jersey, 08544, USA

<sup>3</sup>Interdisciplinary Institute of Light-Element Quantum Materials and Research Center for Light-Element Advanced Materials, Peking University, Haidian, Beijing, 100871, China

Transport measurement, which applies an electric field and studies the migration of charged particles, i.e. the current, is the most widely used technique in condensed matter studies. It is generally assumed that the quantum phase remains unchanged when it hosts a sufficiently small probing current, which is, surprisingly, rarely examined experimentally. In this work, we study the ultra-high mobility two-dimensional electron system using a propagating surface acoustic wave, whose traveling speed is affected by the electrons' compressibility. The acoustic power used in our study is several orders of magnitude lower than previous reports, and its induced perturbation to the system is smaller than the transport current. Therefore we are able to observe the quantum phases become more incompressible when hosting a perturbative current.

Two-dimensional electron systems (2DES) with extremely low disorder host a plethora of exotic quantum many-body states [1–3]. The quantum Hall state (QHS) is incompressible signaled by vanishing longitudinal resistance and quantized Hall resistance [3]. At high Landau level fillings factors  $\nu > 4$ , various charge density waves are stabilized by the large extent of the electron wavefunction [4–6]. The enigmatic 5/2 fractional quantum Hall state (FQHS) attracts tremendous interest [7–16] because its quasi-particles might obey non-Abelian statistics [17–20]. Various of experimental studies are employed to study its topological properties and quasi-particle statistics, such as weak tunneling[21–24], interferometry[25–28], shot noise[29–32] and thermal transport[33–35]. Most of these studies rely upon the hypothesis that a quantum state is unperturbed by the tiny probing current passing through the  $\mu\text{m}$  size device.

Surface acoustic wave (SAW) is a useful current-free technique to investigate the property of 2DES [36–44]. The propagating piezo-electric field accompanying the SAW interacts with the charge carriers, which in turn affects its velocity ( $v$ ) and attenuation. Qualitatively, this interaction is related to the compressibility of 2DES:  $v$  increases when the 2DES becomes incompressible and thus unable to respond to the SAW [45]. In this work, we probe the 2DES using a pW-level, continuous-wave SAW and discover that the  $\sim 100$  nA current flowing through the  $\sim 1$  mm size sample causes a  $\sim 0.1$  ppm (parts per million,  $10^{-6}$ ) increase of the SAW velocity at very low  $T \lesssim 250$  mK. Such a current-induced SAW velocity shift illustrates that a close and careful examination on the charge transport mechanism is essential and imperative.

Our sample is made from a GaAs/AlGaAs wafer grown by molecular beam epitaxy. The 2DES is confined in a 30-nm-wide quantum well, whose electron density is  $2.91 \times 10^{11} \text{ cm}^{-2}$  and low-temperature mobility is about  $2 \times 10^7 \text{ cm}^2/(\text{V}\cdot\text{s})$ . We make a Van der Pauw mesa (length

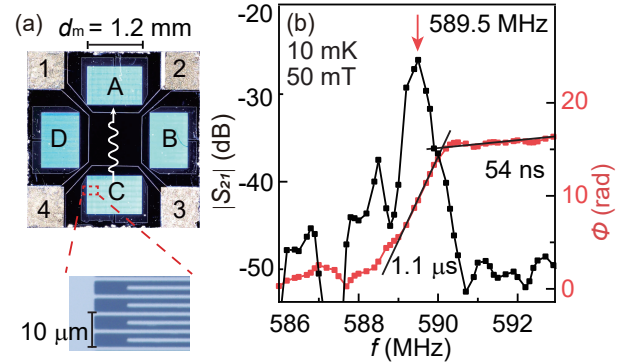


FIG. 1. (a) A photo of our device. The zoom-in plot shows the structure of the aluminum IDT. Two pairs of orthometric IDTs are evaporated on the sample labeled by the alphabets A to D, and four contacts are made at the four corners labeled by numbers 1 to 4. IDT C is used to excite the SAW and IDT A is used for receiving SAW. Unless otherwise specified, the current is injected into contact 1 and flows out from contact 2 while the contact 3 and 4 are float. (b) The measured amplitude ( $|S_{21}|$ ) and phase delay ( $\Phi$ ) of the transmission coefficient as a function of frequency at base temperature  $T$  and magnetic field  $B \sim 50$  mT.

of side  $d_m = 1.2$  mm) by wet etching, and then evaporate 5- $\mu\text{m}$ -period interdigital transducers (IDTs) on each side of the mesa.  $50 \Omega$  resistance is connected in parallel to each IDT for broadband impedance matching. When applied with an AC voltage whose frequency matches the resonance condition, the IDT generates a propagating SAW. The SAW will be captured by the IDT on the opposite side of the sample as a voltage output through the piezoelectric effect [46], see Fig. 1(a).

We use a custom-built superheterodyne demodulation system [47] to analyze the attenuation  $|S_{21}|$  and phase delay  $\Phi$  of the output signal [48]. From the measured  $|S_{21}|$  and  $\Phi$  vs. frequency  $f$  shown in Fig. 1(b), we can

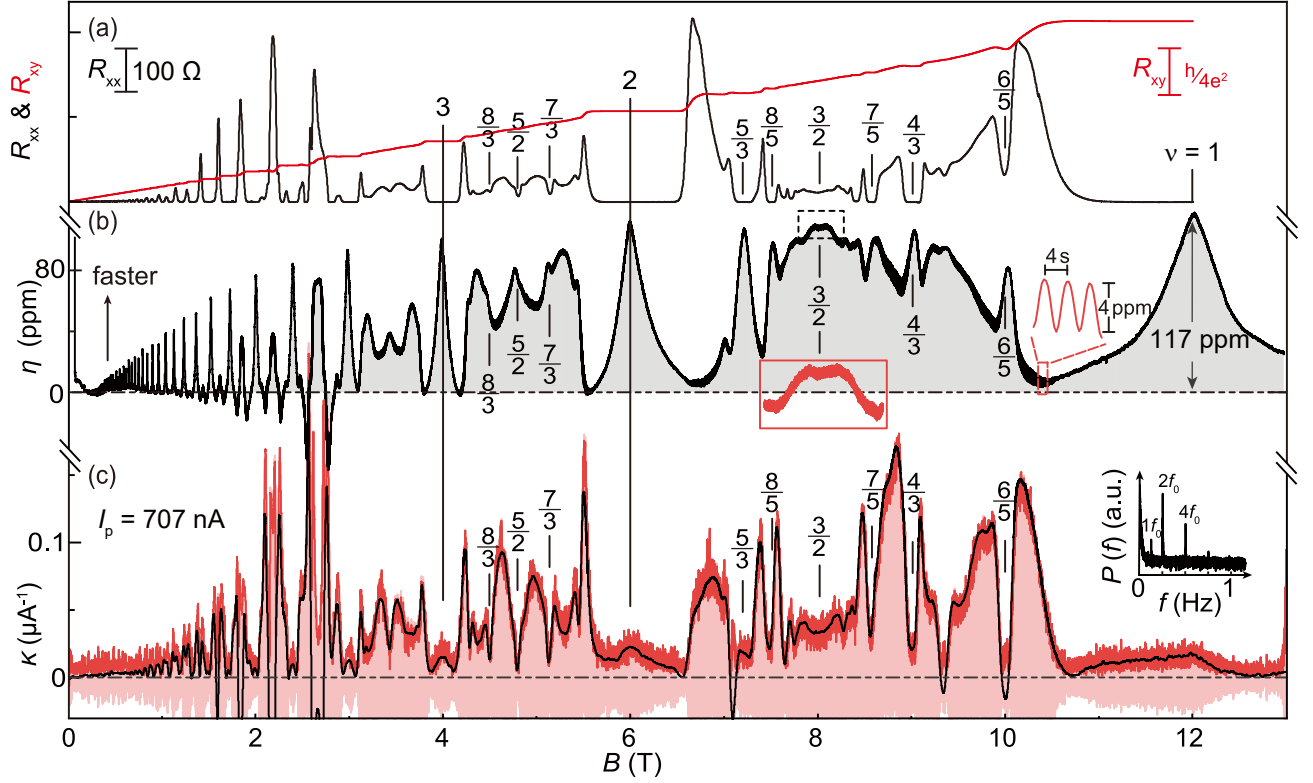


FIG. 2. (a) The longitudinal ( $R_{xx}$ ) and Hall ( $R_{xy}$ ) resistance vs.  $B$ . (b) The measured SAW velocity increase  $\eta(B) = \Delta v(B)/v_0$ . A  $f_0 = 0.125$  Hz,  $I_p = 707$  nA AC current passes through the sample (contact 1  $\rightarrow$  2) during the measurement, imposing a 4-s-period oscillation to  $\eta$ , see the enlarged plot in the red dashed box. Red solid box shows  $\eta$  near  $\nu = 3/2$ . (c) The extracted oscillation using a digital bandpass filter centered at 0.25 Hz (pink curve). Its amplitude can be measured using a lock-in amplifier (black curve). Inset: power spectrum density of the oscillation. The Y coordinate  $\kappa$  is defined as  $\eta_m^{-1} \cdot (\partial\eta/\partial|I|)$ . The meaning of  $\kappa$  is explained in Fig3.

calculate the reference SAW velocity  $v_0$  at low field ( $\simeq 2950$  m/s) from the IDT period ( $5 \mu\text{m}$ ) and the resonant frequency  $f_c$  (589.5 MHz). We can also derive the delay time  $\partial\Phi/\partial(2\pi f) = 1.1 \mu\text{s}$  and 54 ns near and away from the SAW resonance peak, consistent with the  $\sim 3$  mm SAW travel distance and  $\sim 11$ -meter-long coaxial cable (5.5 m each way). The experiment is carried out in a dilution refrigerator whose base temperature is  $\lesssim 10$  mK.

Figure. 2(a) and (b) show the magneto-resistance ( $R_{xx}$ ,  $R_{xy}$ ) and the measured relative SAW velocity increase  $\eta(B) = \Delta v(B)/v_0$ , where  $\Delta v(B) = v(B) - v_0$ . The positive (negative) velocity shift results in the decrease (increase) in the delay time. We can directly deduce  $\eta$  from the measured SAW phase shift  $\Phi$  through  $\eta \simeq -\Delta\tau/\tau = -\Phi/(2\pi f_c\tau)$ , where  $\tau = d_m/v_0 = 407$  ns is the SAW's traveling time through the 2DES. At high  $B$  fields,  $\eta$  exhibits maxima (corresponding to enhanced SAW velocity) when the 2DES forms an incompressible quantum Hall state and its screening capability vanishes [43], see Fig. 2(b). The SAW interacts with 2DES by inducing a screening charge distribution. Therefore  $\eta$  is related to the 2DES compressibility  $\frac{dn}{d\mu}$  [49].  $\eta$  at integer fillings increases monochromatically with decreasing

$\nu$ . We linearly fit the data at  $\nu \lesssim 10$  and define the intercept at  $\nu = 0$  as  $\eta_m = 124$  ppm [49].

Unlike the vanishing plateau seen in  $R_{xx}$ , we observe “V”-shape maxima in  $\eta$ . At the vicinity of integer filling factors  $\nu = N + \nu^*$ ,  $N$  is an integer, the 2DES consists of an incompressible quantum Hall liquid and additional quasiparticles/quasiholes whose filling factor  $|\nu^*| < 1$ . The fact that  $\eta$  has a linear dependence on the quasiparticles/quasiholes density  $n^* = n|\nu^*|/\nu$  suggests that the quantum phase formed by these dilute quasiparticles/quasiholes is compressible [49, 50]. The SAW velocity enhancement is also seen as clear “V”-shape maximum at  $\nu = 4/3, 5/3, 6/5$ , etc., as well as developing maxima at  $\nu = 5/2, 7/3$ , and  $11/5$  where FQHS develop. The SAW velocity enhancement is seen when the SAW propagates along the hard axis of the stripe phase formed at  $\nu = 9/2, 11/2$ , etc., consistent with previous reports [42]. Interestingly,  $\eta$  is large near  $\nu = 3/2$  where the 2DES forms compressible composite Fermion Fermi sea, possibly because the composite Fermions with extremely large effective mass are inert to the SAW-induced field [51].

We are able to reach  $\sim 0.1$  ppm resolution in  $\eta$  while

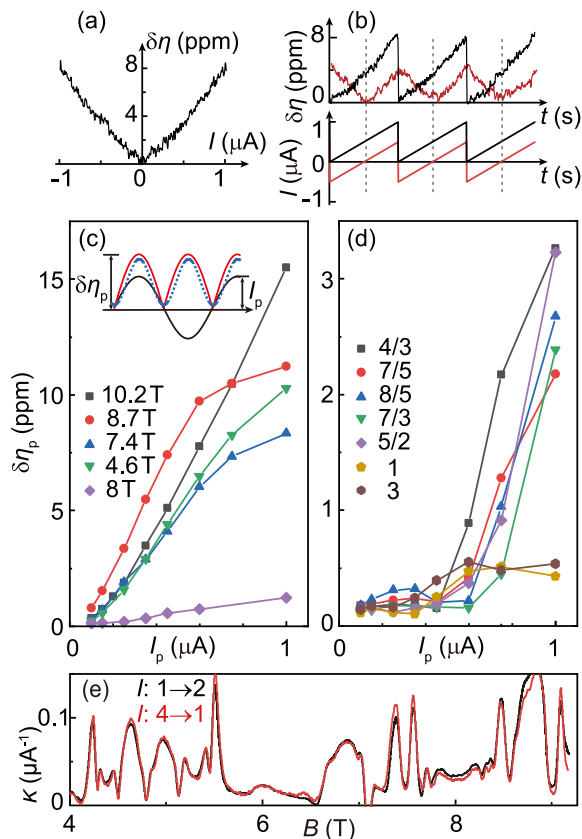


FIG. 3. (a)  $\delta\eta$  vs. DC Current  $I$  at  $B = 4.62$  T. (b)  $\delta\eta$  vs. time measured with different ranges of sweeping current (black and red). (c-d)  $\delta\eta_p$  vs Current peak  $I_p$  at transition states and QHSs. Inset: Black curve is the sinusoidal input current with peak amplitude  $I_p$  and frequency  $f_0$ . Red curve is the current induced velocity shift ( $\delta\eta$ ) with amplitude  $\delta\eta_p$ . Blue dashed curve is the second harmonic component of  $\delta\eta$ . (e)  $\kappa$  vs.  $B$  when current ( $I_p = 707$  nA) flows perpendicular (between contacts 1 & 2) and parallel (4 & 1) to the SAW propagation direction.

using excitation that is orders of magnitude smaller than previous reports [42]. The input RF power in Fig. 2(b) is 1 nW (-61 dBmW) and only a tenth of it turns into SAW considering the attenuation of cables and the efficiency of the IDT. The SAW induced potential on the 2DES is only  $\sim 10$   $\mu\text{eV}$ , leading to  $\lesssim 10^4$   $\text{cm}^{-2}$  electron density fluctuation [49]. Therefore, we can resolve very delicate response of 2DES while preserving the fragile many-body states. One of the most surprising discovery is a velocity shift  $\delta\eta = \eta(B, I) - \eta(B, I = 0)$  induced by a current passing through the 2DES, see Fig. 3(a).  $\delta\eta$  increases nearly linearly by 8 ppm when  $I$  increases from 0 to 1  $\mu\text{A}$ .  $\delta\eta$  is an even function of  $I$ , so that if we sweep the current from -0.5 to 0.5  $\mu\text{A}$ ,  $\eta$  displays a triangle waveform, see Fig. 3(b). We define a parameter  $\kappa = \eta_m^{-1} \cdot (\partial\eta/\partial|I|)$  to describe this current induced velocity shift (CIVS) effect.

We note if the input current is sinusoidal at frequency  $f_0$ , the leading component of  $\delta\eta$  would be the second har-

monic at frequency  $2f_0$ , see the Fig. 3(c) inset. Therefore, we can use lock-in technique to measure amplitude ( $\delta\eta_p$ ) of the  $\delta\eta$  oscillation from its second harmonic [49] and deduce  $\kappa \simeq \eta_m^{-1} \cdot (\delta\eta_p/\delta I_p)$  even when the CIVS effect is small. We measure  $\delta\eta_p$  at different filling factors as a function of the AC current amplitude  $I_p$  in Fig. 3(c) and (d). In the left panel where the 2DES is compressible,  $\delta\eta_p$  increases linearly and then saturates at large current amplitudes. In the right panel, the tiny  $\delta\eta_p$  value does not rise obviously with the increase of current at integer fillings. At fractional fillings, we discover a clear threshold behavior where  $\delta\eta_p$  remains almost zero until  $I_p$  reaches about 600 nA.

The Fig 2(b) data is taken when a  $f_0 = 0.125$  Hz,  $I_p = 707$  nA current passes through the 2DES. In the expanded plot of  $\eta$  in Fig. 2(b) and the power spectrum of the  $\eta$  in the Fig. 2(c), we can clearly observe a 4-s ( $2f_0$ ) period oscillation in  $\eta$ . We apply a digital band-pass filter to the Fig. 2(b) data to extract this oscillation (pink shade) and deduce  $\kappa$  from its amplitude (red trace) in Fig. 2(c). Alternatively, we can use a lock-in amplifier to measure this oscillation amplitude (black trace). The Fig. 2(c) data clearly evidences the dependance of CIVS effect on the quantum phases of 2DES. At strong quantum Hall effects, unlike the “V”-shape maxima in the  $\eta$  trace and the plateau in the  $R_{xx}$  trace,  $\kappa$  presents a “W”-shape minimum – it has a positive peak at exact integer  $\nu = 1, 2, 3$ , etc. and reduces to zero on both sides before increasing. Between  $\nu = 1$  and 2,  $\kappa$  exhibits clear minima at  $\nu = 4/3, 5/3, 7/5, 8/5$  and  $6/5$  when FQHS form, similar to the  $\eta$  and  $R_{xx}$  traces. Surprisingly, clear minimum can be seen in the  $\kappa$  trace corresponding to the fragile FQHS at  $\nu = 5/2, 7/3, 8/3, 11/5$  and  $14/5$  while the  $\eta$  trace only shows a glimmer of maxima.

We can rule out the possibility that finite  $\kappa$  is caused by the heating effect. As discussed in the supplementary,  $\eta$  has little temperature dependence when the sample temperature is below 100 mK. Although there’s no reliable approach to detect the electron temperature of the 2DES, we are quite confident that it is well below 100 mK when taking Fig. 2 data. We can see clear features in  $\eta$  and  $\kappa$  in Fig. 2(b) and (c) for several fragile quantum phases such as the FQHS at  $\nu = 5/2, 7/3$  and  $8/3$  as well as the unidirectional charge density waves at  $\nu = 9/2$  and  $11/2$ , which are only stable at temperatures well below 100 mK. The transport measurements taken using 500 nArms current also shows clear difference when temperature raises to 100 mK [49]. Lastly,  $\kappa$  dip at a fragile QHS such as  $\nu = 5/2$  is much more obvious than the composite Fermion Fermi sea at  $\nu = 3/2$ , although the former is more sensitive to the temperature.

Figure. 4(a) shows that at all fields  $\kappa$  decreases as  $T$  increases, and eventually vanishes when  $T \simeq 250$  mK. The summarized  $\kappa$  vs.  $T$  data at different fields in Fig. 4(b) suggests an exponential dependence  $\kappa \propto \exp(-T/T_C)$  where the characteristic temperature  $T_C$  is about 50 mK

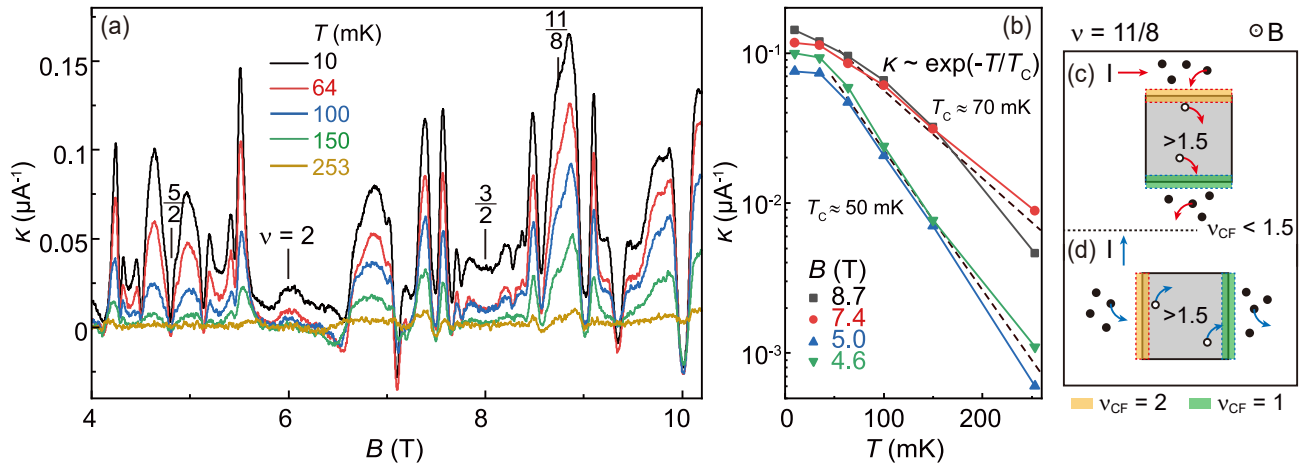


FIG. 4. (a)  $\kappa$  vs.  $B$  at different  $T$ . (b)  $\kappa$  vs.  $T$  at different  $B$ . (c-d) Schematic explanation of the CIVS at  $\nu = 11/8$ . Solid and open dots represent negative-charged quasiparticles and positive-charged quasiholes respectively. (c) and (d) depict situations when currents flow on different directions. The dashed box represents the phase boundary. The grey (white) domain is the region with  $\nu_{CF} > 1.5$  ( $\nu_{CF} < 1.5$ ).

at  $2 < \nu < 3$  and 70 mK at  $1 < \nu < 2$ . More data show that the  $T_c$  is insensitive to the probing SAW frequencies/wavelengths [49]. It is important to mention that the vanishing of  $\kappa$  is unlikely a direct result of reduced quantum Hall stability, since the QHS around  $3/2$  remains quite strong at  $T \simeq 250$  mK when  $\kappa$  vanishes.

The measured  $\kappa$  is almost always positive. The increased SAW velocity suggests that the 2DES becomes more incompressible when carrying current. Intuitively, the current cripples the incompressible phases by introducing more defects/inhomogeneities and broadening the domain walls, so that the 2DES are expected to be more compressible. Also, we observe no changed in  $\kappa$  when we rotate the current direction to be parallel to SAW, see Fig. 3(e), indicating that the CIVS has no dependence on which direction the current flows. Unfortunately, there's very little investigation on the morphing of the quantum phase when carrying a non-destructive current. Meanwhile, the large  $\kappa$  is seen at the transition between two neighboring QHS, where a rigorous description of charge transport mechanism must involve quasiparticle localization and percolation and is particularly hard.

We propose a simple hand-waving mechanism to understand the positive  $\kappa$  in Fig. 4(c). At  $\nu = 4/3$  and  $7/5$ , the electrons in the partially filled Landau level form  $\nu = 1/3$  and  $2/5$  fractional quantum Hall states, respectively, if the 2DES is fully-spin-polarized. These two states can be explained as the  $\nu_{CF} = 1$  and 2 integer quantum Hall states of composite Fermions, and the phase transition happens at  $\nu = 11/8$  when the average composite Fermion filling factor  $\langle \nu_{CF} \rangle = 1.5$ . Because of the density fluctuation [52], the regions with  $\nu_{CF} < 1.5$  ( $\nu_{CF} > 1.5$ ) consist of an incompressible  $\nu = 4/3$  ( $\nu = 7/5$ ) QHS and additional movable negative-charged quasiparticles (positive-charged quasiholes), see

Fig. 4(c). When a current passes through the sample, e.g. from left to right (red arrow), quasiparticles move leftward and quasiholes move rightward. The effective magnetic field poses a Lorentz force, leading to the accumulation and depletion of quasiparticles/quasiholes at the phase boundary. The depletion (accumulation) of quasiholes and accumulation (depletion) of quasiparticles occur at the same boundary, leading to an increase (decrease) in the local density and the formation of incompressible QHS with  $\nu_{CF} = 2$  ( $\nu_{CF} = 1$ ). If we rotate the current to the vertical direction (blue arrow), the incompressible regions rotate as well. In short, the current passing through the disordered 2DES induces incompressible phases at domain boundaries which are always parallel to the current direction. This explains why we measure the same  $\kappa$  in different current directions as shown in Fig. 3(e). Similar discussion can be easily extended to QHS, where the flowing current drives the sparsely distributed, disorder-pinned quasiparticles/quasiholes out of their equilibrium positions and piles them at boundaries of the incompressible liquid phase.

In conclusion, we use the interaction between SAW and electrons to study the morphing of quantum phases in ultra-high mobility 2DES. We discover that the SAW velocity increases, suggesting that the 2DES becomes more incompressible when a non-destructive current flows through the 2DES. This effect is only seen with a revolutionarily enhanced sound velocity resolution at very low temperatures and disappears at  $T \gtrsim 250$  mK.

We acknowledge support by the National Key Research and Development Program of China (Grant No. 2021YFA1401900 and 2019YFA0308403) and the National Natural Science Foundation of China (Grant No. 92065104 and 12074010) for sample fabrication and mea-

surement. The Princeton University portion of this research is funded in part by the Gordon and Betty Moore Foundation's EPiQS Initiative, Grant GBMF9615.01 to Loren Pfeiffer. We thank Xin Wan, Zhao Liu and Bo Yang for valuable discussions.

\* xilin@pku.edu.cn

† liuyang02@pku.edu.cn

- [1] D. C. Tsui, H. L. Stormer, and A. C. Gossard, *Phys. Rev. Lett.* **48**, 1559 (1982).
- [2] R. E. Prange and S. M. Girvin, eds., *The Quantum Hall Effect* (Springer, New York, 1987).
- [3] J. K. Jain, *Composite Fermions* (Cambridge University Press, Cambridge, UK, 2007).
- [4] M. P. Lilly, K. B. Cooper, J. P. Eisenstein, L. N. Pfeiffer, and K. W. West, *Phys. Rev. Lett.* **82**, 394 (1999).
- [5] R. R. Du, D. C. Tsui, H. L. Stormer, L. N. Pfeiffer, K. W. Baldwin, and K. W. West, *Solid State Communications* **109**, 389 (1999).
- [6] A. A. Koulakov, M. M. Fogler, and B. I. Shklovskii, *Phys. Rev. Lett.* **76**, 499 (1996).
- [7] R. L. Willett, J. P. Eisenstein, H. L. Stormer, D. C. Tsui, A. C. Gossard, and J. H. English, *Phys. Rev. Lett.* **59**, 1776 (1987).
- [8] W. Pan, J.-S. Xia, V. Shvarts, D. E. Adams, H. L. Stormer, D. C. Tsui, L. N. Pfeiffer, K. W. Baldwin, and K. W. West, *Phys. Rev. Lett.* **83**, 3530 (1999).
- [9] C. R. Dean, B. A. Piot, P. Hayden, S. Das Sarma, G. Gervais, L. N. Pfeiffer, and K. W. West, *Phys. Rev. Lett.* **101**, 186806 (2008).
- [10] A. Kumar, G. A. Csáthy, M. J. Manfra, L. N. Pfeiffer, and K. W. West, *Phys. Rev. Lett.* **105**, 246808 (2010).
- [11] E. H. Rezayi and F. D. M. Haldane, *Phys. Rev. Lett.* **84**, 4685 (2000).
- [12] M. R. Peterson, T. Jolicoeur, and S. Das Sarma, *Phys. Rev. Lett.* **101**, 016807 (2008).
- [13] A. Wójs, C. Tóke, and J. K. Jain, *Phys. Rev. Lett.* **105**, 096802 (2010).
- [14] R. L. Willett, *Reports on Progress in Physics* **76**, 076501 (2013).
- [15] X. Lin, R. Du, and X. Xie, *National Science Review* **1**, 564 (2014).
- [16] X. Wan, Z.-X. Hu, E. H. Rezayi, and K. Yang, *Phys. Rev. B* **77**, 165316 (2008).
- [17] G. Moore and N. Read, *Nuclear Physics B* **360**, 362 (1991).
- [18] A. Kitaev, *Annals of Physics* **303**, 2 (2003).
- [19] A. Stern, *Nature* **464**, 187 (2010).
- [20] C. Nayak, S. H. Simon, A. Stern, M. Freedman, and S. Das Sarma, *Rev. Mod. Phys.* **80**, 1083 (2008).
- [21] S. Roddaro, V. Pellegrini, F. Beltram, G. Biasiol, L. Sorba, R. Raimondi, and G. Vignale, *Phys. Rev. Lett.* **90**, 046805 (2003).
- [22] J. B. Miller, I. P. Radu, D. M. Zumbühl, E. M. Levenson-Falk, M. A. Kastner, C. M. Marcus, L. N. Pfeiffer, and K. W. West, *Nature Physics* **3**, 561 (2007).
- [23] I. P. Radu, J. B. Miller, C. M. Marcus, M. A. Kastner, L. N. Pfeiffer, and K. W. West, *Science* **320**, 899 (2008).
- [24] H. Fu, P. Wang, P. Shan, L. Xiong, L. N. Pfeiffer, K. West, M. A. Kastner, and X. Lin, *Proc. Natl. Acad. Sci.* **113**, 12386 (2016).
- [25] R. L. Willett, L. N. Pfeiffer, and K. W. West, *Proc. Natl. Acad. Sci.* **106**, 8853 (2009).
- [26] Y. Zhang, D. T. McClure, E. M. Levenson-Falk, C. M. Marcus, L. N. Pfeiffer, and K. W. West, *Phys. Rev. B* **79**, 241304 (2009).
- [27] R. L. Willett, L. N. Pfeiffer, and K. W. West, *Phys. Rev. B* **82**, 205301 (2010).
- [28] J. Nakamura, S. Liang, G. C. Gardner, and M. J. Manfra, *Nature Physics* **16**, 931 (2020).
- [29] L. Saminadayar, D. C. Glatzli, Y. Jin, and B. Etienne, *Phys. Rev. Lett.* **79**, 2526 (1997).
- [30] R. de Picciotto, M. Reznikov, M. Heiblum, V. Umansky, G. Bunin, and D. Mahalu, *Nature* **389**, 162 (1997).
- [31] A. Bid, N. Ofek, H. Inoue, M. Heiblum, C. L. Kane, V. Umansky, and D. Mahalu, *Nature* **466**, 585 (2010).
- [32] M. Dolev, Y. Gross, Y. C. Chung, M. Heiblum, V. Umansky, and D. Mahalu, *Phys. Rev. B* **81**, 161303 (2010).
- [33] W. E. Chickering, J. P. Eisenstein, L. N. Pfeiffer, and K. W. West, *Phys. Rev. B* **87**, 075302 (2013).
- [34] M. Banerjee, M. Heiblum, A. Rosenblatt, Y. Oreg, D. E. Feldman, A. Stern, and V. Umansky, *Nature* **545**, 75 (2017).
- [35] M. Banerjee, M. Heiblum, V. Umansky, D. E. Feldman, Y. Oreg, and A. Stern, *Nature* **559**, 205 (2018).
- [36] A. Wixforth, J. P. Kotthaus, and G. Weimann, *Phys. Rev. Lett.* **56**, 2104 (1986).
- [37] M. A. Paalanen, R. L. Willett, P. B. Littlewood, R. R. Ruel, K. W. West, L. N. Pfeiffer, and D. J. Bishop, *Phys. Rev. B* **45**, 11342 (1992).
- [38] R. L. Willett, R. R. Ruel, K. W. West, and L. N. Pfeiffer, *Phys. Rev. Lett.* **71**, 3846 (1993).
- [39] R. L. Willett, K. W. West, and L. N. Pfeiffer, *Phys Rev Lett* **88**, 066801 (2002).
- [40] B. Friess, V. Umansky, K. von Klitzing, and J. H. Smet, *Phys Rev Lett* **120**, 137603 (2018).
- [41] B. Friess, I. A. Dmitriev, V. Umansky, L. Pfeiffer, K. West, K. von Klitzing, and J. H. Smet, *Phys. Rev. Lett.* **124**, 117601 (2020).
- [42] B. Friess, Y. Peng, B. Rosenow, F. von Oppen, V. Umansky, K. von Klitzing, and J. H. Smet, *Nature Physics* **13**, 1124 (2017).
- [43] I. L. Drichko, I. Y. Smirnov, A. V. Suslov, and D. R. Leadley, *Phys. Rev. B* **83**, 235318 (2011).
- [44] I. L. Drichko, I. Y. Smirnov, A. V. Suslov, Y. M. Galperin, L. N. Pfeiffer, and K. W. West, *Phys. Rev. B* **94**, 075420 (2016).
- [45] Previous work in Ref. [36] explains the velocity shift with the conductivity. Such an analysis may not be suitable here because our ultra-high mobility 2DES has a very long transport scattering time  $\tau_{tr} \simeq 0.7$  ns comparable to the SAW frequency.
- [46] R. M. White and F. W. Voltmer, *Applied physics letters* **7**, 314 (1965).
- [47] M. Wu, X. Liu, R. Wang, X. Lin, and Y. Liu, "A high-performance surface acoustic wave sensing technique," (2023), arXiv:2311.01718 [physics.app-ph].
- [48] See supplementary material for a detailed description of our setup, which includes Refs. [53, 54].
- [49] See supplementary material for more information.
- [50] Y. Chen, R. M. Lewis, L. W. Engel, D. C. Tsui, P. D. Ye, L. N. Pfeiffer, and K. W. West, *Phys. Rev. Lett.* **91**, 016801 (2003).
- [51] Such behavior is surprising but not inconsistent with the

previous report, since our frequency is much lower than the geometric resonance condition [38, 39].

- [52] Y. J. Chung, K. W. Baldwin, K. W. West, N. Haug, J. van de Wetering, M. Shayegan, and L. N. Pfeiffer, *Nano Letters* **19**, 1908 (2019).
- [53] D. Sullivan, D. Allan, D. Howe, and F. Walls, *Inst. Stand. Technol. Technical Note* **1337** (1990).
- [54] P. Durdaut, M. Höft, J.-M. Friedt, and E. Rubiola, *Sensors* **19**, 185 (2019).

## SUPPLEMENTARY MATERIALS

### I. Calibrating our SAW measurement

We introduce a superheterodyne-scheme radio frequency lock-in technique which can measure the phase-shift ( $\Phi$ ) of the delay-line device. The whole setup is optimized for the best phase noise background and stability; see ref. [47] for detailed discussion. A schematic diagram of the system is shown in Fig. S1(a). We use fractional phase-locked-loop (PLL) to generate two single-frequency signals  $V_{\text{in}}$  and  $V_{\text{LO}}$  whose frequencies are linked to the reference clock frequency  $f_{\text{CLK}}$  by  $f_{\text{in}} = \frac{n}{m} \cdot f_{\text{CLK}}$  and  $f_{\text{LO}} = \frac{n+k}{m} \cdot f_{\text{CLK}}$  respectively;  $n$ ,  $m$  and  $k$  are integer values.  $V_{\text{in}}$  is attenuated and sent to the SAW device which attenuates the amplitude by  $\Gamma$  and introduce a phase delay  $\Phi$ . The output signal of the device  $V_{\text{out}}$  will be magnified by a broadband low noise amplifier (LNA) and then multiply with  $V_{\text{LO}}$  at the mixer. We then use a FPGA-based digital lock-in technique to digitize and analyze the differential frequency component  $V_{\text{d}}$ . The I/Q component obtained from the quadrature demodulation is able to deduce the amplitude and phase of  $V_{\text{out}}$ .

We calibrate the measurement system using a delay-line device made from a LiNbO<sub>3</sub> (64°-Y cut) substrate whose center frequency  $f_c$  is 837MHz, see the  $S_{21}$  spectrum in Fig. S1(b). In order to analyze the electronic white noise background, we send a 1 fW (-120 dBm), 837-MHz signal with an on-off modulation using a mechanical switch (10mHz, 70% duty cycle). The demodulation output ( $I$  and  $Q$ ) using resolution bandwidth of about 2 Hz is plotted in Fig. S1(c). When the switch is off, no signal is sent into the device and the demodulation output origins from the leaking signal, resulting in the right cluster of points in Fig. S1(c). When the switch is on, the detected signal is expected to be -155 dBm after attenuated by the cables (about -5dB) and the device (about -30dB), corresponding to the left cluster of points in Fig. S1(c). The two clusters are separated by a distance  $d \simeq 1.29 \mu\text{V}$  and their standard deviation  $\sigma$  is  $0.24 \mu\text{V}$ , consistent with a equivalent -170 dBm electronic noise background. The phase resolution limited by such electrical noise background is  $\delta\theta = \frac{\sigma}{d} = 0.18 \text{ rad}$  at -120 dBm input power, and becomes better than 0.2 mrad when the input signal is about -60 dBm.

We can increase the signal amplitude to increase the phase resolution. However, this enhance has a limit at large signal amplitude when the phase noise of  $V_{\text{in}}$  and  $V_{\text{LO}}$  dominates over the electronic noise [53, 54]. Fig. S1(d) shows the phase noise spectrum at -61 dBm (about 1 nW) input RF power. The measured phase noise spectral density  $S_{\phi}(f)$  is proportional to  $1/f^{0.5}$  at frequencies below  $\sim 1 \text{ Hz}$  (the red solid line), consistent with the frequency jittering of the signal source. It equals about 0.2

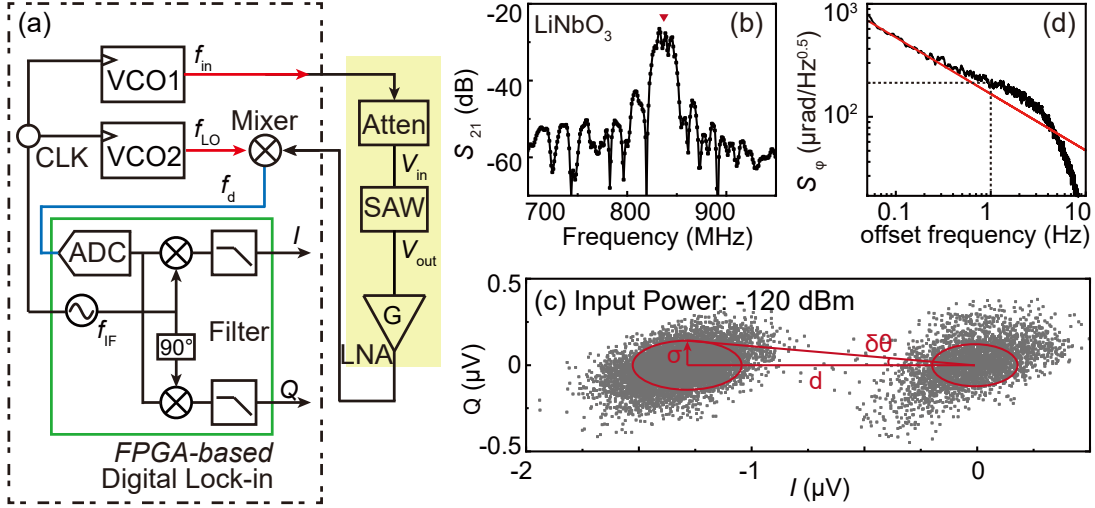


FIG. S1. (a) A simplified diagram of our superheterodyne quadrature phase demodulation system.  $V_{in}$  and  $V_{out}$  are the input and output signal of the device. (b) The  $|S_{21}|$  of the testing LiNbO<sub>3</sub> device measured by our setup as a function of frequency. The device has similar in-band loss compared to the GaAs device used in our main manuscript. (c) The I/Q demodulation output of our setup when the input signal amplitude is -155 dBm, from which we can calibrate the electrical noise floor of our setup is about -170 dBm. (d) The phase noise spectrum of our demodulation output.

mrad/Hz<sup>0.5</sup> at 1 Hz, leading to bounded random phase drift of about 0.3 mrad (i.e. constant Allan deviation).

## II. The temperature response of $\eta$

In this section, we discuss two different mechanism of temperature induced SAW velocity shift.

Usually, the acoustic velocity increases when temperature reduces, and a  $\eta \propto -T^3$  relation is expected in regular materials, e.g. see ref. [47]. At very low temperatures  $T \lesssim 4$  K, we observe a surprising decrease of the SAW velocity in a delay-line sample made from an intrinsic GaAs substrate without any 2DES. The temperature dependence of the SAW velocity shift  $\eta$  of this sample is shown in Fig. S2(a) and (b). Although we have not figure out the mechanism behind this peculiar behavior, we find that  $\eta$  remains basically unchanged at temperatures below 200mK. The electron-phonon coupling becomes extremely weak at temperature below 1 K and the 2DES is believed to be cooled by contacts. It is unlikely that the heat generated by the 500 nA current passing through the high mobility 2DES, which is less than 1 nW, can heat up the lattice to above 50 mK. Furthermore, the heating power of this current is roughly proportional to magnetic field, because the 2-point resistance of these ultra-high mobility 2DES is approximately  $R_{xy}$  at magnetic fields  $B \gtrsim 0.5$  T. This is also inconsistent with the oscillating behavior of our measured  $\kappa = \eta_m^{-1} \cdot (\partial\eta/\partial|I|)$ .

Besides the lattice effect, the quantum phase in 2DES itself is also sensitive to temperature so that  $\eta$  can also be influenced. In Fig. S2(c), we show the  $\eta$  vs.  $B$  measured

at different temperatures. The traces taken at different temperature are offset so that the  $\eta$  peak at strong integer quantum Hall effects such as  $\nu = 1, 2$  and 3 as well as at low magnetic field  $B \simeq 0$  T, which is assumed to be insensitive to temperatures, are aligned. The Fig. S2(d) shows  $\eta$  at  $B = 10.2$  T where the largest temperature dependence is seen.  $\eta$  has a linear dependence on  $T$  and  $d\eta/dT$  is about 0.2 ppm/mK, and saturates below about 70 mK. Therefore, it is only possible to achieve the  $\simeq 10$  ppm amplitude of  $\delta\eta_P$  if the 2DES is heated up to about 120 mK. On the other hand, we show  $R_{xx}$  measured using 500 nA current in Fig. S2(e). At  $\nu = 9/2$  and  $\nu = 11/2$ , where the spontaneous unidirectional charge density wave phase is stabilized, a clear difference in  $R_{xx}$  is seen when the mixing chamber temperature raises from 64 mK to 100 mK, suggesting that the 2DES temperature is below 100 mK if the 500 nA passing through the device at fridge base temperature. Therefore the heating effect of 2DES is unlikely the leading cause of the large current-induced increase in the sound velocity.

## III. Electron density fluctuation

In this section, we provide a rough estimation of the electron density fluctuation of 2DES induced by SAW. The SAW speed  $v_0 \simeq 2950$  m/s is much smaller than the Fermi velocity of charged quasiparticles ( $v_F \simeq 3 \times 10^5$  m/s), and the transport scattering time is of the same order as the SAW period. We can assume that the response of 2DES to the SAW-induced electric field is fast enough so that the 2DES is almost always at equilibrium

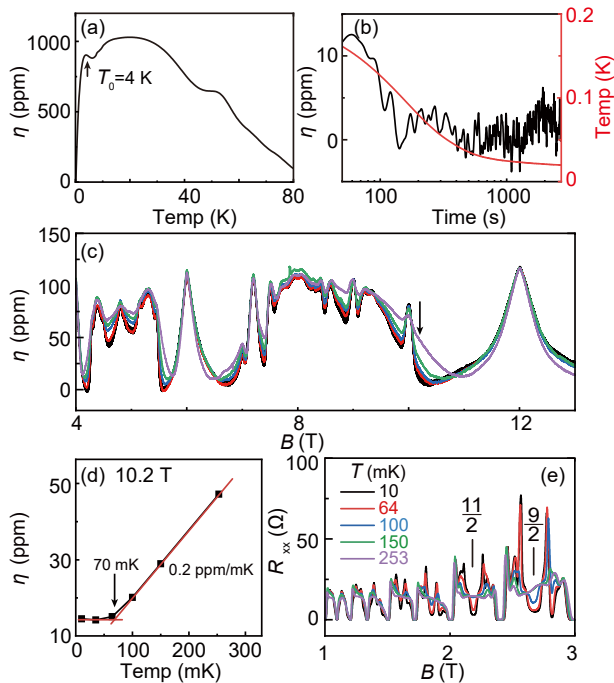


FIG. S2. (a) SAW velocity shift  $\eta$  of an intrinsic GaAs sample as a function of the temperature  $T$ . The SAW velocity increases as temperature decreases at relative high temperatures  $T \gtrsim 4$  K. (b) The SAW velocity decreases i.e.  $\eta$  reduces, when temperature decreases from 4K to 200mK, and remains unchanged at temperatures below about 200 mK. (c)  $\eta$  vs.  $B$  at different Temperatures. (d) The  $\eta$  vs. Temperature  $T$  at  $B = 10.2$  T shows a linear increasing of  $\eta$  at temperatures above 70 mK. (e)  $R_{xx}$  taken near filling factors  $\nu = 9/2$  and  $11/2$  using 500 nA measurement current at different temperatures. The  $R_{xx}$  minima at  $\nu = 9/2$  and  $11/2$  signal the formation of unidirectional charge density waves, whose temperature dependence suggests that the 2DES remains below 100 mK when 500 nA current passing through the device.

and the problem can be solved statically. The propagating piezoelectric field introduced by SAW at a given time (e. g.  $t = 0$ ) is

$$\vec{E}_{\text{ext}} = \vec{E} \cdot \cos(-\omega t + kx)|_{t=0} = \vec{E} \cdot \cos(kx) \quad (1)$$

where  $k$  denotes the wavevector of the SAW. We then have the SAW-induced external potential is

$$\Phi_{\text{ext}} = - \int \vec{E}_{\text{ext}}(x) dx = - \frac{E}{k \sin(kx)} \quad (2)$$

Using Thomas-Fermi screening model, the induced charge is

$$\rho_{\text{ind}} = -e^2 \cdot \frac{dn}{d\mu} \Phi_{\text{scr}} / D \quad (3)$$

where  $\frac{dn}{d\mu}$  is the 2DES's compressibility, i.e. the density of state at Fermi energy for Fermi sea. And we assume

the 2DES as a flat plate of uniform thickness  $D = 20$  nm and neglect the stray field. The screened potential  $\Phi_{\text{scr}}$  is the sum of the external potential and the induced potential

$$\Phi_{\text{scr}} = (\Phi_{\text{ind}} + \Phi_{\text{ext}}) \quad (4)$$

$\Phi_{\text{ind}}$  can be calculated from  $\rho_{\text{ind}}$  using the Gaussian law

$$\nabla^2 \Phi_{\text{ind}} = -\rho_{\text{ind}} / \epsilon_0 \epsilon_r \quad (5)$$

Combining the above relations, the induced potential can be deduced by the following equation self-consistently.

$$\nabla^2 \Phi_{\text{ind}} = e^2 \frac{dn}{d\mu} \frac{1}{D \epsilon_0 \epsilon_r} (\Phi_{\text{ind}} + \Phi_{\text{ext}}) \quad (6)$$

It is easy to see that

$$\Phi_{\text{ind}} = - \frac{\Phi_{\text{ext}}}{1 + \frac{D \epsilon_0 \epsilon_r k^2}{e^2 \frac{dn}{d\mu}}} \quad (7)$$

In GaAs  $\epsilon_r = 13.1$ , the density of state in 2DES at zero field is  $\frac{dn}{d\mu} = \frac{m_e}{2\pi\hbar^2}$ . The induced potential cancels the external potential if  $\frac{D \epsilon_0 \epsilon_r k^2}{e^2 \frac{dn}{d\mu}} \ll 1$ . We can deduce the induced electron density.

$$n_{\text{ind}} = -\rho_{\text{ind}} \cdot D / e = \epsilon_0 \epsilon_r \nabla^2 \Phi_{\text{ind}} \cdot D / e = \frac{D \epsilon_0 \epsilon_r k^2 \Phi_{\text{ext}}}{e} \quad (8)$$

If the 2DES is incompressible, i.e.  $dn/d\mu = 0$ ,  $\Phi_{\text{ind}}$  and  $n_{\text{ind}}$  are both zero and the interaction between 2DES and SAW vanishes. The induced electrons with  $n_{\text{ind}}$  propagate along with the SAW. The power dissipation and phase delay of SAW occur when induced electrons are scattered by impurities or the quasiparticle velocity is comparable or less than the SAW velocity.

$\Phi_{\text{ext}}$  can be estimated from the signal amplitude received by the output IDT. In our experiment as shown by the inset of Fig. S3, the typical input RF power is -61 dBm (about 1 nW) and the output is about -97 dBm. The cable attenuation is about -5 dB at 600 MHz so that the power at the output IDT is -92 dBm. The IDT capacitance  $C_{\text{IF}} \sim 20$  pF corresponds to  $\sim 10 \Omega$  impedance at 600 MHz, sufficiently small to be neglected. We can estimate that the voltage at the receiving IDT is about 10  $\mu\text{V}$ , leading to  $\sim 10^4 \text{ cm}^{-2}$  electron density fluctuation, orders of magnitude smaller than the density fluctuation of the 2DES itself ( $\sim 10^9 \text{ cm}^{-2}$  even in very high-mobility samples [52]).

In the experiment, the SAW excitation power (-61 dBm) is a trade-off between the principle of "non-perturbative" measurement and the signal-to-noise ratio (SNR). Namely, the power should be sufficiently low so that  $n_{\text{ind}}$  is negligible, while it should be large enough to resolve interesting phenomena. The proper input power

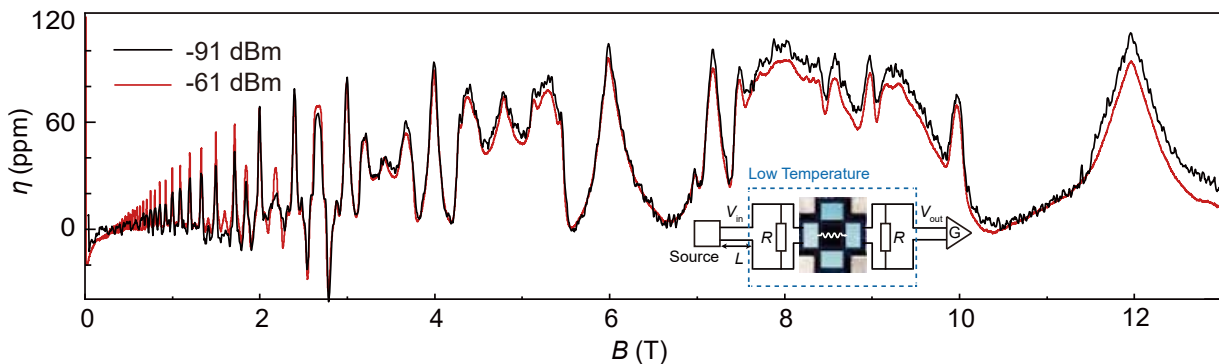


FIG. S3. SAW velocity shift  $\eta$  measured under different input SAW powers. Inset: Schematic diagram of the measurement setup. The IDT is connected in parallel with a  $50 \Omega$  resistance ( $R$ ). The coaxial cable ( $L \sim 5.5$  m) is connected from the base temperature to room temperature.

is chosen by the following rationale. We first measure  $\eta$  using the lowest possible power, e.g.  $-91$  dBm which corresponds to  $n_{\text{ind}} \sim 300 \text{ cm}^{-2}$ . We then increase the power to  $-61$  dBm. We find that the measured two  $\eta$  are almost identical, see Fig. S3, suggesting that  $-61$  dBm is sufficiently low. The power received by our lock-in amplifier is about  $-92$  dBm. Our setup has  $-170$  dBm noise background when using  $300$  ms time constant (corresponds to about  $0.3$  Hz effective noise bandwidth). The  $80$  dB SNR ratio leads to about  $0.1$  ppm resolution in  $\eta$ , sufficiently high for this study.

#### IV. $\eta$ near integer fillings

Near the integer Landau level filling factors  $\nu = N$ , we observe “V”-shape maxima instead of plateaus in  $\eta$ . This might be related to the finite compressibility of Wigner crystal formed by the dilute quasiparticles/quasiholes whose effective filling factor  $\nu^* = |\nu - N|$  is small [50]. In Fig. S4(a), we observe a linear dependence between  $\eta$  and the effective quasi-particle density  $n^* = n|\nu^*|/\nu$ .

$\eta$  at exact integer fillings  $\nu = N$  increases when the quantum Hall state becomes stronger. We summarize  $\eta$  at different integer filling in Fig. S4(b).  $\eta$  has a rather linear dependence on  $\nu$  at  $\nu < 10$ , whose intercept at  $\nu = 0$  is about  $\eta_m = 124.2$  ppm.  $\eta_m$  marks the maximum effect the 2DES poses on the SAW and can be used to normalization  $\kappa$ .

#### V. The origin of the second harmonics

As shown in Fig. 3 of the manuscript, the SAW velocity shift is proportional to the amplitude of current. Therefore, an AC current passing through the sample

$$I = I_p \sin(\omega t) \quad (9)$$

induces a SAW velocity shift

$$\delta\eta = \delta\eta_p |\sin(\omega t)| = \eta_m \kappa I_p |\sin(\omega t)| \quad (10)$$

The Fourier series of  $\delta\eta$  can be expanded as

$$\delta\eta = \delta\eta_p \left( \frac{4}{\pi} - \frac{4}{3\pi} \cos(2\omega t) - \dots - \frac{2(1 + (-1)^n)}{(n^2 - 1)\pi} \cos(n\omega t) \right) \quad (11)$$

where  $n$  is a non-negative even integer. The dominate component of the signal is second harmonics, whose amplitude is

$$\delta\eta_{2f} = \delta\eta_p \cdot \frac{4}{3\pi} \quad (12)$$

Therefore, we can measure  $\delta\eta_{2f}$  and deduce  $\delta\eta_p$ . We can also deduce  $\kappa$  by

$$\kappa = \frac{1}{\eta_m} \frac{\partial \eta_p}{\partial I_p} = \frac{3\pi}{4\eta_m} \frac{\partial \eta_{2f}}{\partial I_p} \quad (13)$$

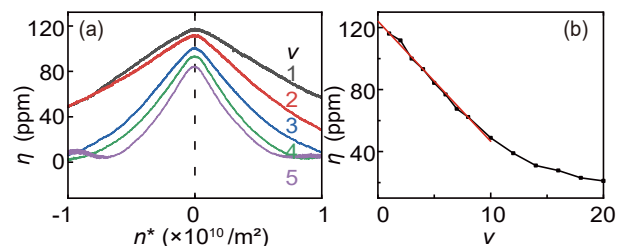


FIG. S4. (a)  $\eta$  vs effective electron density  $n^*$  at different integer fillings. (b) The linear relationship between  $\eta$  and  $\nu$ .

#### VI. Data using lower SAW frequency

We repeat the acoustic study in another sample. The IDT period  $\lambda$  is  $12 \mu\text{m}$  and the SAW resonance frequency

is  $f_c = 243.1$  MHz. The primary feature of  $\kappa$  in this device (see Fig. S5) is similar to the data reported in the main text. Similarly,  $\kappa$  decreases with increasing temperature and finally vanishes when  $T \simeq 250$  mK. We conclude that the phenomena we reported in the manuscript have no dependence on the SAW frequency and wavelength.

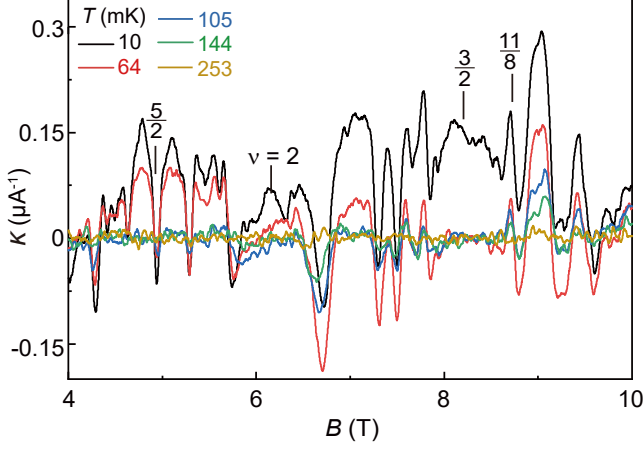


FIG. S5.  $\kappa$  vs magnetic field at different temperatures of another sample with lower resonance frequency (243.1 MHz). The IDT period  $\lambda$  is 12  $\mu\text{m}$ .

### VII. Data from a lower mobility sample

For comparison, we perform similar acoustic study on a lower mobility sample. The electron density of the 2DES is  $1.12 \times 10^{11} \text{ cm}^{-2}$  and its low-temperature mobility is about  $1.14 \times 10^6 \text{ cm}^2/(\text{V}\cdot\text{s})$ .  $\eta \approx 700$  ppm at  $\nu = 1$  is larger in this sample, because the 2DES is shallower and the interaction between 2DES and SAW is stronger. Thanks to this large  $\eta$ , we can measure  $\delta\eta$  directly with DC current, similar to the Fig. 3(a) data in the main text. The threshold current is about 200 nA for both the  $\nu = 1$  QHS and the  $\nu = 2/3$  FQHS, see Fig. S6(a). Therefore, integer and fractional QHS exhibit similar CIVS if the quasiparticles are randomly localized and no Wigner crystal exists.

Fig. S6(b) shows  $\delta\eta$  as a function of the DC current

$I$  at  $\nu = 1$ .  $\delta\eta$  increases when the current increases above the threshold. It saturates at large current  $I > 2 \mu\text{A}$ . Meanwhile, the differential longitudinal resistance increases by less than a percent, signaling that the integer QHS is still far below breakdown.

### VIII. Device fabrication

The samples are  $5 \times 5$  mm square cleaved directly from a GaAs/AlGaAs wafer grown via molecular beam

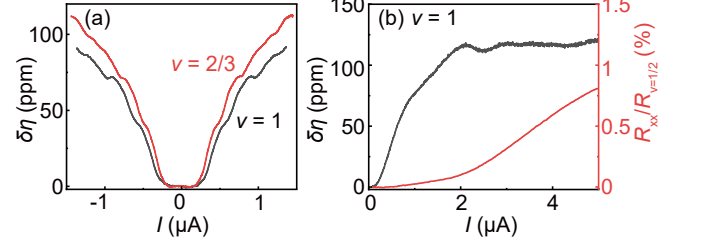


FIG. S6. In the lower mobility sample, (a)  $\delta\eta$  vs. DC Current  $I$  at  $\nu = 1$  (black curve) and  $\nu = 2/3$  (red curve). (b)  $\delta\eta$  (black curve) and normalized differential longitudinal resistance ( $R_{xx}/R_{\nu=1/2}$ ) (red curve) vs. large DC Current  $I$  at  $\nu = 1$ . The differential longitudinal resistance is measured under small AC current and normalized by the longitudinal resistance at  $\nu = 1/2$ .

epitaxy. The 30-nm-wide quantum well locates at 390 nm below the surface. We use three  $\delta$ -doping layers, the deepest one is about 80 nm below the quantum well. The low temperature mobility of the 2DES is about  $2 \times 10^7 \text{ cm}^{-2}/(\text{V}\cdot\text{s})$ .

We make ohmic contacts at the four corners of the sample by depositing Ge/Au/Ni/Au alloy and annealing at 440  $^{\circ}\text{C}$  for 30 minutes. A  $d_m = 1.2$  mm square Van der Pauw mesa is then created by wet etching using a  $\text{H}_2\text{O}:\text{H}_2\text{O}_2:\text{H}_2\text{SO}_4$  solution (240:8:1) for 4 minutes. The etching depth is approximately 800nm. We pattern the interdigital transducers (IDTs) with evaporated 400  $\text{\AA}$  Al using a maskless laser lithography system and lift-off process. Each IDT has 170 pairs of fingers with a periodicity of  $\lambda = 5 \mu\text{m}$ . The center-to-center spacing of opposite pair of IDTs is 2450  $\mu\text{m}$ .